Article

A Wide-Field Optical Coherence Tomography Normative Database Considering the Fovea-Disc Relationship for Glaucoma Detection

Hyungjun Kim[1,2], Jong Sub Lee[1,3], Hae Min Park[1,3], Hyunsoo Cho[1], Han Woong Lim[1,3], Mincheol Seong[1,3], Junhong Park[2], and Won June Lee[1,3]

[1] Department of Ophthalmology, Hanyang University College of Medicine, Seoul, Korea
[2] Department of Mechanical Engineering, Hanyang University, Seoul, Korea
[3] Department of Ophthalmology, Hanyang University Seoul Hospital, Seoul, Korea

Correspondence: Won June Lee, Department of Ophthalmology, Hanyang University College of Medicine, Department of Ophthalmology, Hanyang University Seoul Hospital, 222-1, Wangsimni-ro Seongdong-gu, 04763, Seoul Korea. e-mail: wonjunelee@hanyang.ac.kr

Purpose: One purpose of this study was to collect wide-field swept-source optical coherence tomography (SS-OCT) data from healthy eyes and build a wide-filed normative database. Another purpose was to compare the glaucoma diagnostic ability of new parameters based on this normative database to the parameters that are currently in use, such as the peripapillary retinal nerve fiber layer (RNFL), macular ganglion cell-inner plexiform layer, and ganglion cell complex (GCC) thickness.

Methods: This study had 220 healthy eyes and 292 eyes with early-stage glaucoma (EG) and moderate-stage glaucoma (MG) enrolled. Using the wide-field SS-OCT images (12 × 9 mm) of healthy eyes, a wide-field normative database was constructed by transforming and combining the individual images into a uniform template using the fovea and optic disc centers as fixed landmarks. Adjustment for the disc size was conducted. With this normative database, new parameters based on the ratio of the fovea-disc distance (FDD) consisting of the fovea-disc relationship were evaluated. The glaucoma diagnostic ability was assessed based on the area under the receiver operating characteristic curve (AUC).

Results: Among the new peripapillary parameters, the RNFL of the circumference of the circle with diameter 0.8 FDD showed the highest AUC value for EG and MG, but the value was not significantly superior to that of the initial RNFL (AUC = 0.940 vs. 0.937, P = 0.631). Among the macular parameters, the GCC of the area of the circle of 1.5 FDD showed the highest AUC value for EG and MG, and the value was significantly superior to that of initial GCC (AUC = 0.929 vs. 0.919, P = 0.033). However, there was no significant difference between the initial and adjusted GCC thickness in patients included in the EG or MG groups separately.

Conclusions: A wide-field normative database was built to consider the relationship between the fovea and the optic disc. Considering this aspect, we found that the GCC analysis using a broader area presented a significantly greater glaucoma diagnostic performance for EG and MG in the macula than the initial parameter for the GCC.

Translational Relevance: Based on this wide-field normative database, the clinical use of a wide-field deviation map may help diagnose the patients with EG and MG in the future.

Introduction

Optical coherence tomography (OCT) has been widely used to diagnose glaucoma,[1–4] and ophthal-mologists can confirm structural changes in eyes with glaucoma more objectively using this advanced hardware and software. In addition to the classical observation of the retinal nerve fiber layer (RNFL) around the optic disc head (peripapillary), the macular

1

inner retinal structure has received attention in the field of glaucoma.[5–7] Recently, studies on the temporal sequences and spatial relations between the peripapillary and macular areas[8–11] have been published. Some studies have suggested that it may be useful to diagnose glaucoma to integrate these two areas using advanced hardware (i.e. wide-field scan with swept-source technology)[12,13] and software (i.e. scan individually and combine each area).[8,9]

For glaucoma diagnosis, the thicknesses of the peripapillary RNFL (pRNFL) and the macular inner retinal structure are used, including the ganglion cell-inner plexiform layer (mGCIPL) or ganglion cell complex (mGCC). The deviation map, which compares the patients' thickness data with an embedded normative database in each sector, is used as well.[14,15] At present, the analysis is performed in each peripapillary and macular area separately without considering them together, even though these two areas are connected to each other. The axon bundles from the ganglion cells at the macular area all converge together around the optic disc, which is not reflected in the analysis. For example, even though the axis connecting the fovea and the optic disc can vary for each individual,[16] a normative database was collected with reference to the horizontal meridian. Uniform parameters, such as a circle with a radius of 3.4 mm from the center of the optic disc or a circle with a radius of 6.0 mm from the macula, are used even though the distance between the fovea and the optic disc varies from person to person.

Because wide-field images covering the fovea and macula area together are possible through swept-source OCT (SS-OCT), we collected wide-field OCT data from healthy subjects using imaging technology and built a wide-field normative database considering the fovea-disc relationship. Our study will devise new parameters that reflect the relationship between the two areas and compare the diagnostic ability of these new parameters to that of parameters being currently used for early and moderate glaucoma.

Methods

The study protocol was approved by the Institutional Review Board of Hanyang University Hospital (institutional review board [IRB] number: HYUH 2020-03-035-001). The study design followed the tenets of the Declaration of Helsinki for biomedical research.

Subjects

For this retrospective cross-sectional study, we enrolled 512 eyes: 220 healthy eyes, 220 eyes with early glaucoma (EG), and 72 eyes with moderate-stage glaucoma (MG). All participants visited the Glaucoma Clinic of Hanyang University Hospital between August 2019 and February 2020. All the subjects underwent a complete ophthalmologic examination, including visual acuity testing, manifest refraction assessment, slit-lamp examination, intraocular pressure measurements using Goldmann applanation tonometry, gonioscopy, dilated fundus examination, axial length measurement (IOL Master; Carl Zeiss Meditec, Dublin, CA, USA), stereo disc photography, and red-free RNFL photography (EIDON confocal scanner; CenterVue, Padua, Italy), Swedish interactive thresholding algorithm 24-2 perimetry (Humphrey Field Analyzer II; Carl Zeiss Meditec, Jena, Germany), and SS-OCT (DRI-OCT Triton; Topcon, Tokyo, Japan).

A visual field was considered reliable if the fixation losses were <20%, the false positive rate was <15%, and the false-negative rate was <15%. A normal visual field was defined as a mean deviation (MD) and pattern standard deviation (PSD) within 95% confidence limits, and a glaucoma hemifield test (GHT) result within normal limits. Eyes with glaucomatous visual field defects were defined as those with a cluster of 3 points with probabilities of <5% on the pattern deviation map in at least 1 hemifield, including at least 1 point with a probability of <1%; or a cluster of 2 points with a probability of <1%; and a GHT result outside 99% of age-specific normal limits or a PSD outside 95% of normal limits. The visual field defects were confirmed on two consecutive reliable tests.[17]

The inclusion criteria were a best-corrected visual acuity of 20/40 or better, spherical equivalent refractive errors between +6.0 diopter (D) and −6.0 D, cylinder correction <3.0 D, and open anterior chamber angle. The exclusion criteria were as follows: a history of ophthalmic surgery (e.g. glaucoma-filtering surgery), severe glaucoma showing a MD worse than −12 dB, any other ocular disease that could interfere with the visual function, any media opacity that would significantly interfere with acquisition of OCT images, and an inability to obtain a high-quality OCT image (i.e. Image Quality scores <50). For cases in which both the eyes met all the eligibility criteria, one eye was randomly chosen as the study eye.

Patients with open-angle glaucoma were identified by several signs in addition to an open angle confirmed on gonioscopy. The first sign is the presence of a characteristic optic disc defined as a localized or diffuse neuroretinal rim thinning, increased cupping, or a cup-to-disc ratio difference >0.2 between the eyes on a stereo disc photograph. The presence of RNFL defect on red-free fundus imaging was an alternative sign,

regardless of the presence or absence of glaucomatous visual field defects.

Based on visual field test results, patients with preperimetric glaucoma (normal visual field) and early perimetric glaucoma (visual field loss with MD ≥ -6 dB) were enrolled as the EG group, and those with a visual field loss with MD between -6 dB and -12 dB were enrolled as the MG group. Healthy eyes were defined as those of patients with no history or evidence of intraocular surgery, intraocular pressure ≤ 21 mm Hg with no history of increased intraocular pressure, the absence of glaucomatous disc appearance, and normal ophthalmologic findings. A wide-field OCT scan analysis was performed according to the right-eye orientation.

Two glaucoma specialists (W.J.L. and M.S.), who were masked to all other patient information, independently evaluated all the photographs. In cases of disagreement, the cases were excluded to avoid ambiguity.

Swept-Source Optical Coherence Tomography

A wide-field scan protocol (12×9 mm) was applied using a DRI-OCT. The DRI-OCT is an SS-OCT device that uses a wavelength-sweeping laser with a center wavelength of 1050 nm and a tuning range of approximately 100 nm. We acquired 100,000 A-scans with an 8-µm axial resolution in tissue per second. The 12×9-mm scan contained 256 B-scans, each containing 512 A-scans for a total of 131,072 axial scans/volume. This method has been described in detail previously.[13]

Construction of Wide-Field Normative Database

The overall explanation of the method used for constructing the wide-field normative database is described in Supplementary Figure S1. The wide-field data was standardized as a unified template to consider the fovea-disc relationship and the size of the discs. The raw data of the thickness value allocated at each pixel were extracted from the built-in software as an Excel file. The dimension of the wide-field OCT image was 12×9 mm, which was set to have 512 and 256 evenly spaced points, respectively. We used MATLAB R2019b (The MathWorks, Inc., Natick, MA) for all image analysis. Each coordinate of the wide-field scan was transformed by zooming in, zooming out, and rotating it based on the fovea-disc relationship so that all optic disc and macular centers have the same points.

We converted the thickness data by the transformed coordinate matched to the initial coordinate using the linear interpolation. After that, to consider the size of the disc, it is assumed that the coordinate corresponding to the disc margin was stretched or shrank, and the amount of deformation at the disc margin decreased linearly from the disc margin to the center of the macula. The thickness data was converted again by the transformed coordinate matched to the initial coordinate using the linear interpolation. Through this process, each data with the same optic disc and macular centers could be constructed as maintaining the initial coordinates. Detailed methods of the entire process are described below.

To consider the fovea-disc relation, all optic discs and macular centers need to coincide with each other. The center of the optic disc was arbitrarily chosen as (8.3, 4.5), such that the fovea-disc diameter (FDD) was 4.5 mm and the fovea-disc angle (FDA) was 6 degrees. Based on these two points, the initial coordinates were zoomed in, zoomed out, and rotated with FDD = 4.5 mm and FDA = 6 degrees. As shown in Supplementary Figure S2, if the optic discs and macular centers in the initial coordinate are A and B, respectively, the FDD in the initial coordinate can be expressed as $|\overrightarrow{BA}|$. If the optic and macular centers in the transformed coordinate are A′ and B′, respectively, the FDD in the transformed coordinate (FDD′) can be expressed as $|\overrightarrow{BA'}|$. The coordinates zoomed in and out from the optic center can be expressed as:

$$\begin{aligned} x' &= \tfrac{\text{FDD}'}{\text{FDD}} x - R_x \\ y' &= \tfrac{\text{FDD}'}{\text{FDD}} y - R_y \end{aligned} \qquad (1)$$

where R_x and R_y are the x and y directional components of vector, R, in Supplementary Figure S2. The coordinates rotated with θ at the optic disc center as shown in Supplementary Figure S3 may be represented by:

$$\begin{pmatrix} x' \\ y' \end{pmatrix} = \begin{pmatrix} \cos\theta & \sin\theta \\ -\sin\theta & \cos\theta \end{pmatrix} \begin{pmatrix} x \\ y \end{pmatrix} \qquad (2)$$

In order to standardize the thicknesses data zoomed in, out, and rotated from the Equations 1 and 2, all the coordinates of the thicknesses (coordinates of pixels) needed to be identical. Linear interpolation was used to obtain the thicknesses data corresponding to the initial coordinates.

To consider the size of the disc of each patient, it is assumed that the coordinate corresponding to the disc margin was stretched or shrank at the same disc margin, which was set to have a diameter of 1.6 mm according to the average disc size of the patients in this

study. The amount of deformation at the disc margin decreased linearly from the disc margin to the center of the macula. To understand this process, the transformed coordinate is shown in Supplementary Figure S4 with an example case.

We converted the wide-field data to the template obtained for each patient using this method. Based on this, the thicknesses of the RNFL, GCC, and GCIPL on the circle were measured after drawing a circle with a diameter of the distance (0.6, 0.7, 0.8, 0.9, and 1.0) proportional to the FDD, rather than a constant distance from the center of the optic disc. Around the macula, a circle with a diameter of the distance proportional to the FDD (1.3, 1.35, 1.4, 1.45, and 1.5) was drawn, and the thicknesses of the GCC and GCIPL in that circle were measured. The ability to diagnose glaucoma using these new parameters was calculated, and the most superior diagnostic parameters were chosen to describe the wide-field normative database.

We developed a normative database only for normal groups by selecting a parameter found to have the most superior diagnosis ability for glaucoma. The average, bottom 5%, and 1% values were obtained and are presented. The 12-hour sectors around the optic disc center and 6 sectors around the macular center were divided in consideration of the FDA. The ability to diagnose glaucoma in each sector was also analyzed.

In a subanalysis, the diagnostic abilities of the new parameters in discriminating eyes with EG or MG from healthy eyes were separately evaluated.

Statistical Analyses

Statistical tests were performed using IBM SPSS Statistics 24 (IBM Corp, Armonk, NY) and MedCalc (MedCalc Software, Ostend, Belgium). To compare the characteristics, the independent *t*-test was used for continuous variables and the χ^2 test was used for categoric variables. The area under the receiver operating characteristic curves (AUCs) was calculated for continuous parameters, and comparison of AUC values between parameters was assessed using the method described by DeLong et al.[18] In addition, sensitivities at fixed specificities of 80% and 95% were calculated. All statistical analyses, including the AUCs and sensitivities at fixed specificities, were analyzed in the healthy and glaucoma (EG + MG) groups and separately analyzed in eyes with EG and MG. The *P* values < 0.05 were considered statistically significant. The values were recorded and are presented as mean ± standard deviation.

Results

A total of 512 eyes (220 healthy eyes, 220 eyes with EG, and 72 eyes with MG) that met the inclusion criteria were included in this study.

Clinical Demographics

Table 1 shows the clinical demographics of all patients at the time of enrollment. Between the healthy and glaucoma groups, the differences in age, intraocular pressure, spherical equivalent, FDD, and FDA, were not significant. On the other hand, there were differences between the two groups in MD, PSD, visual field index, and pRNFL, mGCIPL, and mGCC thicknesses (healthy versus glaucoma, *P* < 0.001).

Comparison of Glaucoma Diagnostic Power in the Combination of Early and Moderate Glaucoma

Among the new peripapillary parameters, the pRNFL of the circumference of the circle with diameter 0.8 FDD (pRNFL 0.8 FDD) showed the highest AUC value (AUC = 0.940), but the value was not significantly superior to that of the initial pRNFL thickness (AUC = 0.937, *P* = 0.631; Table 2). All the peripapillary parameter sensitivities at fixed specificities of 95% and 80% are presented in Table 2.

Using macular parameters, new GCC parameters adjusted with the ratio of the FDD showed larger AUC values than that of initial mGCC, which showed the highest diagnostic power among the initial parameters. Among them, the mGCC thickness of the area of the circle of 1.5 FDD (mGCC 1.5 FDD) showed the highest AUC value (AUC = 0.929), and the value was significantly superior to that of the initial mGCC thickness (AUC = 0.919, *P* = 0.033; Table 3). All the macular parameter sensitivities at fixed specificities are presented in Table 3. A larger diameter may result in higher sensitivities at fixed specificities. Moreover, the result at mGCC 1.5 FDD was higher than the initial result (adjusted versus initial sensitivities at 95% specificity, 71.6% vs. 66.1%).

From the above-mentioned results, the pRNFL 0.8 FDD and mGCC 1.5 FDD, which showed the highest diagnostic power, were selected among the new parameters. With these selected parameters, sectors were classified in each part in consideration of the FDA (12-hour sectors around the optic disc and 6 sectors in the macula), and the diagnostic power for the EG in these new sectors is presented in Table 4.

Table 1. Clinical Demographic Characteristics of Enrolled Patients

	Total	Healthy	Glaucoma	Early Glaucoma	Moderate Glaucoma	P Value[*]	P Value[**]
	(N = 512)	(N = 220)	(N = 292)	(N = 220)	(N = 72)		
Age, y	57.3 ± 15.3	56.2 ± 16.6	58.1 ± 14.2	57.7 ± 14.9	59.6 ± 12.2	0.173	0.234
Gender (male)	269 (52.5)	116 (52.7)	153 (52.4)	117 (53.2)	36 (50.0)	0.941	0.893
IOP, mm Hg	15.2 ± 3.3	15.3 ± 3.2	15.0 ± 3.2	15.0 ± 3.2	15.2 ± 3.1	0.259	0.470
Spherical equivalent	−1.34 ± 2.60	−1.22 ± 2.60	−1.43 ± 2.60	−1.51 ± 2.48	−1.21 ± 2.93	0.374	0.470
Axial length	24.28 ± 1.32	24.11 ± 1.20	24.38 ± 1.38	24.49 ± 1.46	24.04 ± 0.99	0.205	0.151
MD	−3.92 ± 3.24	−1.42 ± 1.80	−4.47 ± 3.47	−2.90 ± 1.93	−9.03 ± 2.77	<0.001	<0.001
PSD	3.75 ± 2.83	1.87 ± 0.83	4.36 ± 3.06	3.04 ± 1.83	8.31 ± 2.63	<0.001	<0.001
VFI	92.5 ± 8.9	98.3 ± 2.5	90.8 ± 9.7	94.9 ± 4.7	78.9 ± 10.7	<0.001	<0.001
FDD	4.66 ± 0.29	4.66 ± 0.28	4.67 ± 0.30	4.67 ± 0.29	4.65 ± 0.32	0.673	0.784
FDA	7.08 ± 3.78	7.08 ± 3.77	7.08 ± 3.80	7.05 ± 3.50	7.15 ± 4.64	0.995	0.980
pRNFL thickness, μm	92.1 ± 18.2	107.1 ± 9.5	80.8 ± 14.7	84.7 ± 12.9	69.0 ± 13.7	<0.001	<0.001
mGCIPL thickness, μm	65.0 ± 8.5	71.4 ± 5.0	60.1 ± 7.3	61.9 ± 6.1	54.8 ± 8.2	<0.001	<0.001
mGCC thickness, μm	99.3 ± 12.6	109.2 ± 6.9	91.9 ± 10.7	94.5 ± 9.2	84.1 ± 11.0	<0.001	<0.001

Data are mean ± standard deviation or number (%).

[*]Comparisons of *P* values were performed between the Healthy and Glaucoma groups (the chi-square test for categorical variables and the independent t test for continuous variables).

[**]Comparisons of *P* values were performed among the healthy, early glaucoma, and moderate glaucoma groups (the χ^2 test for categorical variables and 1-way ANOVA for continuous variables).

MD, mean deviation; PSD, pattern standard deviation; VFI, visual field index; FDD, fovea-disc diameter; FDA, fovea-disc angle; pRNFL, peripapillary retinal nerve fiber layer; mGCIPL, macular ganglion cell–inner plexiform layer; mGCC, macular ganglion cell complex.

Table 2. Diagnostic Abilities of Peripapillary Parameters in Discriminating Glaucoma (Early and Moderate) Based on Area Under the Curve Values

	Total (N = 512)	Healthy (N = 220)	Glaucoma (N = 292)	P Value*	AUC	P Value**	Sensitivity At 95% Specificity	Sensitivity At 80% Specificity
pRNFL thickness, µm	92.1 ± 18.2	107.1 ± 9.5	80.8 ± 14.7	<0.001	**0.937 (0.913 to 0.957)**		76.5	88.5
pRNFL 0.6 FDD, µm	106.3 ± 22.4	124.6 ± 13.1	92.6 ± 17.7	<0.001	0.932 (0.906 to 0.952)	0.439	70.2	88.0
pRNFL 0.7 FDD, µm	95.1 ± 19.1	110.8 ± 10.6	83.3 ± 15.1	<0.001	0.937 (0.912 to 0.956)	0.946	71.9	91.1
pRNFL 0.8 FDD, µm	84.7 ± 16.7	98.5 ± 9.3	74.3 ± 13.2	<0.001	**0.940 (0.916 to 0.959)**	0.631	72.6	90.8
pRNFL 0.9 FDD, µm	75.7 ± 14.9	87.9 ± 8.4	66.4 ± 11.8	<0.001	0.938 (0.913 to 0.957)	0.953	72.6	90.8
pRNFL 1.0 FDD, µm	68.6 ± 13.6	79.7 ± 7.9	60.2 ± 10.8	<0.001	0.934 (0.909 to 0.954)	0.681	69.5	89.7
pGCIPL 0.6 FDD, µm	39.7 ± 6.7	42.3 ± 6.0	37.7 ± 6.4	<0.001	0.697 (0.655 to 0.736)	<0.001	15.4	45.6
pGCIPL 0.7FDD, µm	40.2 ± 5.9	42.1 ± 5.1	38.8 ± 6.0	<0.001	0.664 (0.622 to 0.705)	<0.001	17.8	44.5
pGCIPL 0.8 FDD, µm	40.5 ± 5.6	42.2 ± 4.7	39.3 ± 5.9	<0.001	0.660 (0.617 to 0.701)	<0.001	14.7	37.3
pGCIPL 0.9 FDD, µm	41.0 ± 5.6	42.6 ± 4.6	39.8 ± 6.0	<0.001	0.659 (0.617 to 0.700)	<0.001	12.7	38.0
pGCIPL 1.0 FDD, µm	41.7 ± 5.7	43.5 ± 4.6	40.3 ± 6.1	<0.001	0.677 (0.634 to 0.717)	<0.001	16.1	43.2
pGCC 0.6 FDD, µm	146.0 ± 26.4	166.9 ± 16.3	130.2 ± 21.1	<0.001	0.923 (0.897 to 0.945)	0.094	67.1	87.3
pGCC 0.7 FDD, µm	135.3 ± 22.2	152.8 ± 13.5	122.2 ± 17.9	<0.001	0.922 (0.895 to 0.944)	0.061	71.2	88.4
pGCC 0.8 FDD, µm	125.2 ± 19.7	140.6 ± 12.2	113.6 ± 16.0	<0.001	0.919 (0.892 to 0.941)	0.039	65.4	88.7
pGCC 0.9 FDD, µm	116.7 ± 18.0	130.6 ± 11.4	106.2 ± 14.8	<0.001	0.913 (0.885 to 0.936)	0.013	63.7	86.0
pGCC 1.0 FDD, µm	110.3 ± 17.0	123.1 ± 10.8	100.6 ± 14.1	<0.001	0.908 (0.879 to 0.931)	0.006	61.6	86.3

Data are mean ± standard deviation.

* Comparisons of P values were performed with the χ^2 test for categorical variables and the independent *t*-test for continuous variables.

** Comparisons of P values were performed with the method described by DeLong et al. for AUC comparison (comparison with pRNFL thickness).

AUC, area under the receiver operating characteristic curve; pRNFL, peripapillary retinal nerve fiber layer; pGCIPL, peripapillary ganglion cell – inner plexiform layer; pGCC, peripapillary ganglion cell complex; FDD, fovea-disc diameter.

Table 3. Diagnostic Abilities of Macular Parameters in Discriminating Glaucoma (Early and Moderate) Based on Area Under the Curve Values

	Total (N = 512)	Healthy (N = 220)	Glaucoma (N = 292)	P Value*	AUC	P Value**	Sensitivity At 95% Specificity	Sensitivity At 80% Specificity
mGCC thickness, µm	99.3 ± 12.6	109.2 ± 6.9	91.9 ± 10.7	<0.001	**0.919 (0.892 to 0.941)**		66.1	83.6
mGCIPL thickness, µm	65.0 ± 8.5	71.4 ± 5.0	60.1 ± 7.3	<0.001	0.907 (0.879 to 0.931)	0.100	60.6	83.2
mGCC 1.3 FDD, µm	98.0 ± 12.4	107.6 ± 6.9	90.8 ± 10.6	<0.001	0.916 (0.888 to 0.938)	0.409	65.4	84.3
mGCC 1.35 FDD, µm	97.4 ± 12.4	107.1 ± 6.8	90.1 ± 10.5	<0.001	0.920 (0.893 to 0.942)	0.873	66.1	86.0
mGCC 1.4 FDD, µm	96.9 ± 12.4	106.7 ± 6.8	89.5 ± 10.4	<0.001	0.923 (0.896 to 0.944)	0.341	68.8	86.6
mGCC 1.45 FDD, µm	96.4 ± 12.5	106.4 ± 6.8	88.9 ± 10.4	<0.001	0.925 (0.899 to 0.947)	0.118	69.9	86.6
mGCC 1.5 FDD, µm	95.9 ± 12.6	106.1 ± 6.8	88.3 ± 10.4	<0.001	**0.929 (0.903 to 0.949)**	0.033	**71.6**	**87.0**
mGCIPL 1.3 FDD, µm	64.1 ± 8.5	70.3 ± 5.6	59.4 ± 7.2	<0.001	0.888 (0.858 to 0.914)	<0.001	55.8	81.5
mGCIPL 1.35 FDD, µm	62.8 ± 8.2	68.9 ± 5.5	58.2 ± 7.0	<0.001	0.887 (0.857 to 0.913)	<0.001	55.5	81.2
mGCIPL 1.4 FDD, µm	61.5 ± 8.1	67.4 ± 5.4	57.1 ± 6.8	<0.001	0.886 (0.856 to 0.913)	<0.001	53.4	80.8
mGCIPL 1.45 FDD, µm	60.2 ± 7.9	66.0 ± 5.4	55.9 ± 6.6	<0.001	0.885 (0.854 to 0.911)	<0.001	51.4	81.5
mGCIPL 1.5 FDD, µm	59.0 ± 7.8	64.6 ± 5.4	54.7 ± 6.4	<0.001	0.882 (0.850 to 0.908)	<0.001	49.7	81.2
mRNFL 1.3 FDD, µm	33.9 ± 5.0	37.3 ± 3.4	31.4 ± 4.4	<0.001	0.862 (0.829 to 0.890)	<0.001	60.6	77.7
mRNFL 1.35 FDD, µm	34.6 ± 5.2	38.3 ± 3.7	31.9 ± 4.6	<0.001	0.869 (0.837 to 0.897)	<0.001	61.6	78.4
mRNFL 1.4 FDD, µm	35.4 ± 5.5	39.3 ± 3.7	32.4 ± 4.8	<0.001	0.877 (0.845 to 0.904)	<0.001	62.0	80.1
mRNFL 1.45 FDD, µm	36.2 ± 5.8	40.4 ± 3.8	33.0 ± 5.0	<0.001	0.884 (0.853 to 0.910)	0.002	63.0	81.7
mRNFL 1.5 FDD, µm	37.0 ± 6.1	41.5 ± 4.0	33.6 ± 5.2	<0.001	0.890 (0.860 to 0.916)	0.010	64.0	82.9

Data are mean ± standard deviation

* Comparisons of P values were performed with the χ^2 test for categorical variables and the independent t-test for continuous variables.

** Comparisons of P values were performed with the method described by DeLong et al. for AUC comparison (comparison with mGCC thickness).

AUC, area under the receiver operating characteristic curve; mRNFL, macular retinal nerve fiber layer; mGCIPL, macular ganglion cell – inner plexiform layer; mGCC, peripapillary ganglion cell complex; FDD, fovea-disc diameter.

Table 4. Diagnostic Abilities of Parameters in Discriminating Glaucoma Based on Area Under the Curve Values

	Total (N = 512)	Healthy (N = 220)	Glaucoma (N = 292)	P Value[*]	AUC	P Value[**]	Sensitivity At 95% Specificity	Sensitivity At 80% Specificity
pRNFL thickness, μm								
7 o'clock	118.7 ± 42.8	150.3 ± 22.5	94.9 ± 38.9	<0.001	0.889 (0.858 to 0.915)		67.5	82.4
11 o'clock	118.9 ± 37.0	140.8 ± 20.0	102.5 ± 38.3	<0.001	0.842 (0.807 to 0.872)	0.010	59.4	73.3
6 o'clock	124.8 ± 39.3	150.3 ± 28.3	105.6 ± 35.4	<0.001	0.837 (0.802 to 0.868)	0.007	48.6	69.8
pRNFL 0.8 FDD thickness adjusted by FDA, μm								
7 o'clock	121.3 ± 41.8	153.3 ± 19.9	97.2 ± 37.6	<0.001	0.904 (0.875 to 0.928)	0.116	67.5	83.6
11 o'clock	104.2 ± 31.1	124.0 ± 19.5	89.2 ± 29.7	<0.001	0.834 (0.799 to 0.865)	0.002	54.5	73.6
12 o'clock	113.2 ± 34.8	135.2 ± 27.7	96.7 ± 30.2	<0.001	0.823 (0.788 to 0.855)	0.006	40.1	65.8
mGCC thickness, μm								
Inferotemporal sector	87.8 ± 14.7	99.2 ± 6.6	79.2 ± 13.1	<0.001	0.916 (0.889 to 0.939)		75.0	85.4
Inferior sector	95.4 ± 16.1	107.5 ± 7.6	86.3 ± 14.8	<0.001	0.905 (0.877 to 0.929)	0.180	70.9	85.6
Superotemporal sector	88.5 ± 11.9	96.7 ± 6.5	82.3 ± 11.3	<0.001	0.879 (0.847 to 0.906)	0.005	63.0	82.0
mGCC 1.5 FDD thickness adjusted by FDA, μm								
Inferotemporal sector	82.8 ± 13.4	93.3 ± 6.7	74.8 ± 11.6	<0.001	0.913 (0.885 to 0.936)	0.668	74.0	86.0
Inferior sector	94.2 ± 16.1	106.7 ± 8.1	84.8 ± 14.1	<0.001	0.910 (0.882 to 0.933)	0.541	71.6	86.0
Superotemporal sector	80.6 ± 11.2	88.7 ± 7.4	74.6 ± 9.7	<0.001	0.881 (0.850 to 0.908)	0.020	55.1	81.5

Data are mean ± standard deviation.

[*] Comparisons of P values were performed with the χ^2 test for categorical variables and the independent t-test for continuous variables.

[**] Comparisons of P values were performed with the method described by DeLong et al. for AUC comparison (comparison with 7 o'clock pRNFL thickness/ inferotemporal mGCC thickness).

AUC, area under the receiver operating characteristic curve; mRNFL, macular retinal nerve fiber layer; mGCIPL, macular ganglion cell – inner plexiform layer; mGCC, peripapillary ganglion cell complex; FDD, fovea-disc diameter.

Table 5. *P* Values for Testing Differences in AUROC

	pRNFL	pRNFL 0.8 FDD	mGCC	mGCC 1.5 FDD	mGCIPL
(AUROC)	(0.937)	(0.940)	(0.919)	(0.929)	(0.907)
pRNFL	NA	.631	0.107	0.438	**0.007**
pRNFL 0.8 FDD	0.631	NA	**0.046**	0.219	**0.003**
mGCC	0.107	**0.046**	NA	**0.033**	0.100
mGCC 1.5 FDD	0.438	0.219	**0.033**	NA	**0.004**
mGCIPL	0.007	**0.003**	0.100	**0.004**	NA

The *P* values are shown and the values of *P* < 0.05 are presented as boldface numbers. The method described by DeLong et al. was used for the AUC comparison.

AUC = area under the receiver operating characteristic curve; mRNFL = macular retinal nerve fiber layer; mGCIPL = macular ganglion cell – inner plexiform layer; mGCC = peripapillary ganglion cell complex; FDD = fovea-disc diameter

The new sector parameters did not show significantly superior diagnostic power compared to previously defined sectors. Table 5 shows a comparison of the AUCs of the best parameters using initial and adjusted methods.

Comparison of Glaucoma Diagnostic Power According to Glaucoma Stage

In the EG, among the new peripapillary parameters, the pRNFL 0.8 FDD showed the highest AUC value (AUC = 0.925), but the value was not significantly superior to that of initial pRNFL thickness (AUC = 0.920, P = 0.573; Supplementary Table S1). Among the new macular parameters, mGCC 1.5 FDD showed the highest AUC value (AUC = 0.909), but the value was not significantly superior to that of the initial mGCC thickness (AUC = 0.898, P = 0.054; Supplementary Table S2). In the case of mGCC, a larger diameter resulted in higher sensitivities at fixed specificities. Moreover, the result at mGCC 1.5 FDD was higher than the initial result (adjusted versus initial sensitivities at 95% specificity, 64.6% vs. 58.2%).

In MG, among the new peripapillary parameters, the pRNFL 0.7 FDD showed the highest AUC value (AUC = 0.991), but the value was not significantly superior to that of the initial pRNFL thickness (AUC = 0.989, P = 0.600; Supplementary Table S3). The sensitivity at fixed specificity at pRNFL 0.7 FDD was higher than the initial ones (adjusted versus initial sensitivities at 95% specificity, 97.2% vs. 94.4%). Among the new macular parameters, the mGCC 1.5 FDD showed the highest AUC value (AUC = 0.988), but the value was not significantly superior to that of the initial mGCC thickness (AUC = 0.983, P = 0.186; Supplementary Table S4). In the case of mGCC, a larger diameter resulted in higher sensitivities at fixed specificities. Especially, the result at mGCC 1.5 FDD was higher than the initial result (adjusted versus initial sensitivities at 95% specificity, 93.1% vs. 90.3%).

Wide-Field Normative Database

The wide-field normative database is presented in Figure 1 and Table 6. The initial (at 3.4-mm circle based on the horizontal line) and adjusted (at the 0.8 FDD circle in consideration of FDA) TSNIT plots of the pRNFL thickness were compared and are presented in Figure 2. The angle with the thickest pRNFL was 72 degrees and −72 degrees before the adjustment and 78 degrees and −63 degrees after the adjustment.

Discussion

First, the FDD and FDA definitions and measurements have a fundamental limitation. This is because the actual eyeball is three-dimensional, but the wide-field SS-OCT images we have obtained are two-dimensional. Consequently, we should assume that we are analyzing two-dimensional images. In addition, as Hood et al. showed, the analysis starts with the assumption that the axon from the ganglion cells of the macular area enters the optic disc area through a certain path, and there is a spatial relationship between the two areas.[6,19]

In the case of the pRNFL, the method considering FDD and the size of the disc did not show higher diagnostic power than the initial method. However, because, theoretically, axons from a similar number of cells gather into the optic disc, the distance between the optic disc and the macula (FDD) may influence the measurement of the axon thickness. It would be more logical to draw a circle with the FDD ratio adjusted for each patient rather than using an empirical distance of 3.4 or 3.5 mm from the optic disc center. The RNFL
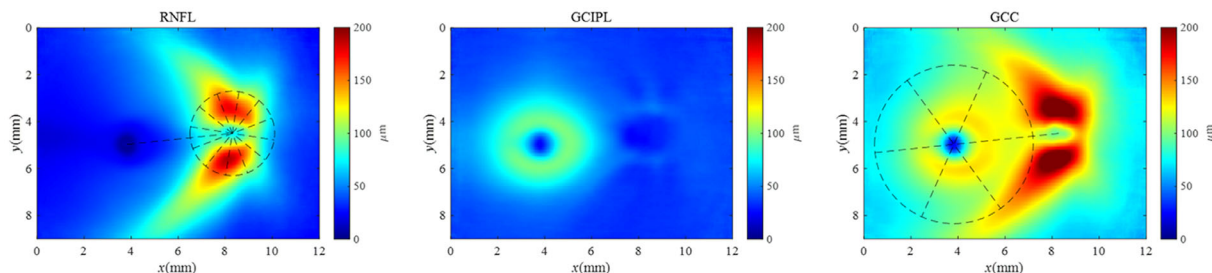
Figure 1. **Wide-field normative database considering the fovea-disc relationship**. The wide-field data is standardized as a unified template to consider the fovea-disc relationship. The average thickness of the retinal nerve fiber layer (RNFL), ganglion cell – inner plexiform layer (GCIPL), and ganglion cell complex (GCC) of wide-field is presented.

is thinner farther away from the optic disc than it is closer to the disc.[20] The distance from the optic disc margin to the measured circle has also been reflected in this study through the adjustment according to the size of the disc.[21] Although there was no statistical difference in diagnostic power, it may be more logical to use parameters reflecting the FDD and disc area rather than a constant of 3.4 mm. Additionally, different blood vessel positions may have different effects on each individual[22,23]; however, this was ignored to construct an average normative database.

After finding the optimal peripapillary distance considering the FDD, the peripapillary area was divided into 12-hour sectors adjusted for the FDA. Previously, Mwanza et al. conducted a similar study considering the FDA using the PanoMap (Cirrus OCT),[24] and Spectralis OCT software draws a peripapillary TSNIT graph through an axis considering fovea-Bruch's membrane opening (BMO).[16] In this study, the diagnostic ability of new peripapillary sectors was not significantly different from those of 12-hour sectors divided based on the horizontal line, which did not reflect the FDA. Our results are consistent with those of a previous study that adjusted the parameters according to the FDA using the Cirrus OCT data but did not improve glaucoma detection performance.[25] Recently, one study reported the RNFL assessment adjusting for anatomic confounders, including the optic disc (ratio, orientation, and area), fovea (distance and angle), and retinal vessel density. In that study, the authors reported that it can reduce the variability of measurements and improve the glaucoma diagnostic ability. They also assert that anatomic compensation should be considered when refining the RNFL normative database.[23] Those efforts are consistent with the purpose of our research.

In the macular area, the mGCC showed the highest AUC value among the initial parameters. As the adjustment was performed through the FDD, the mGCC showed excellent diagnostic power among the RNFL, GCIPL, and GCC in the macular area. As the circle size from the center of the macula increased, the AUC value increased. In the case of the 1.5 FDD, the diagnostic power was significantly higher than the initial mGCC thickness in the 6.0-mm circle. Even when the sensitivity at fixed specificity was compared, it was observed that the value gradually increased as the circle size increased.

The damage beyond the macular scan size or beyond the 6 × 6-mm square where the normative database of the macula was built has not been detected as glaucomatous structural damage in the conventional OCT deviation map. Therefore, superior or infero-inferior damage of the optic disc was detected only in the peripapillary area because the RNFL runs along a distinct path far from the macula so that damage was not detected in the macular area. As a result, we found a discrepancy between these two areas. This issue can be overcome with a wide-field deviation map in the future. The large scan size of the macular area showed high glaucoma diagnostic ability in this study because the larger area could cover these parts, unlike in the initial method.

A recent study analyzing the association between the FDD and macular parameters of healthy subjects showed that eyes with a great FDD are prone to false-positive classification in the thickness assessment of the macular inner retinal layers. Thus, the thickness should always be interpreted in the context of the FDD.[26] The results of the study are also consistent with the efforts of our research. We attempted to draw a larger circle but did not determine when the circle is bigger than the 1.5 FDD because many cases exceed the 12 × 9-mm scan area. These measurements should be considered if the wider area can be scanned to develop future OCT technologies.

Even when the macula was divided into sectors, we saw no significant increase in diagnostic power after adjusting for the FDA. In dividing the macular sector, the temporal raphe could be more meaningful than the

Table 6. Wide-Field Normative Database Considering the Relationship Between the Fovea and the Disc

The Peripapillary Retinal Nerve Fiber Layer Thickness at the Circumference of the Circle With Diameter 0.8 Fovea-Disc Distance

	12	1	2	3	4	5	6	7	8	9	10	11	Average
Mean	135.2	113.6	86.5	62.1	61.6	91.4	123,1	153.3	90.1	62.3	83.5	124.0	98.5
5%	90.3	73.4	51.6	45.3	44.4	59.2	79.3	119.1	67.9	50.9	65.6	93.2	83.4
1%	81.1	56.6	29.8	17.3	34.9	51.8	67.3	112.0	62.1	46.8	61.1	86.7	78.6

The Macular Ganglion Cell Complex Thickness at the Area of the Circle With Diameter 1.5 Fovea-Disc Distance

	Superonasal (SN)	Superior	Superotemporal (ST)	Inferotemporal (IT)	Inferior	Inferonasal (IN)	Average
Mean	120.3	103.0	88.7	93.3	106.6	124.7	106.1
5%	106.2	91.0	76.2	83.2	94.7	109.3	92.2
1%	100.3	88.5	68.4	79.1	90.8	107.2	94.5

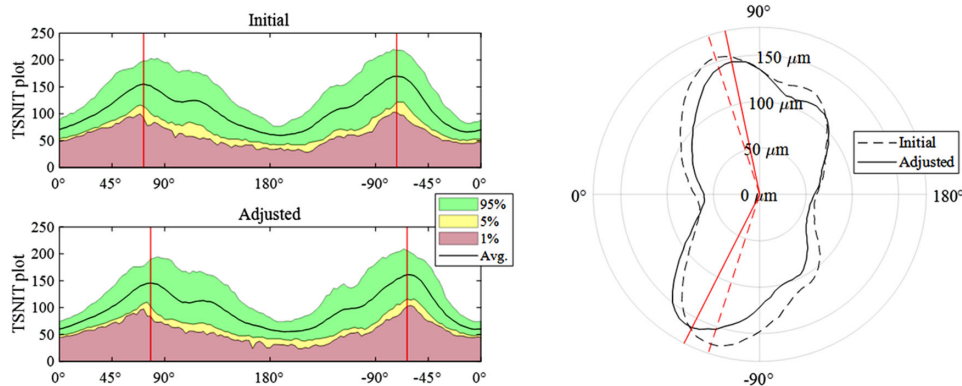All directions are based on the fovea-disc angle.

Figure 2. Original (at 3.4-mm circle based on the horizontal line) and adjusted (at the 0.8 FDD circle in consideration of FDA) TSNIT plots of peripapillary retinal nerve fiber layer thickness. The angle with the thickest peripapillary retinal nerve fiber layer was 72 degrees and −72 degrees before adjustment and 78 degrees and −63 degrees after adjustment.

fovea-disc positional relationship.[27] A previous study reported that the orientation of the temporal raphe is not maintained according to the fovea-BMO axis or the horizontal meridian. Further research is needed on this aspect. Previously, one study corrected the fovea-disc inclination while performing a grid-wide analysis of the macular area. However, in that study, compensation for the fovea-disc inclination did not improve the diagnostic capability.[28]

In this study, we excluded the patients with severe glaucoma showing a MD worse than 12 dB. The reason is that the detection of early structural damage is important in less advanced-stage glaucoma. In advanced glaucoma, diffuse damage may be found, and the damage can be easily diagnosed using any method. We performed the subanalyses evaluating the diagnostic abilities of glaucoma, separately in the EG and MG groups. The diagnostic abilities of new parameters were not statistically superior to those of initial parameters in both stages. However, for the RNFL and GCC in the macular area, the AUC values increased as the analysis range widened in both stages.

Unlike the analysis of the combination of two groups, in the subanalysis of each group, no statistically significant results were found from the adjusted methods, in which the macular scan size increased. In the case of the EG group, the AUC result showed a substantially significant *P* value of 0.054. It may be hypothesized that the number of samples increased in the case that had advantage considering the wider area and the possibly higher statistical significance. Analysis on each group (EG or MG) might not show a significant *P* value because the samples were not enough. If we combined both groups, the number of samples would have been increased and, therefore, a significant *P* value could have been obtained.

The proposed method in this study has two main strengths. First, this wide-field approach considered the spatial relation between the fovea and the optic disc. This is to logically challenge the initial uniformed peripapillary 3.4-mm circle, macular 6.0-mm circle, and peripapillary 12-hour analysis or deviation map square based on horizontality. Although more logical parameters were suggested in our study, consideration of the FDD and FDA did not show a significant improvement in the diagnostic power. Second, the larger area is used for the analysis. The advantages were found when analyzing a wider area than the initial one, especially in the macula area. This may be the answer to the need for a wide-field related software or a wide-field normative database in keeping with the evolution of the wide-field SS-OCT hardware. Our group has reported the advantages of the wide-field RNFL thickness map and also reported the advantage of the wide-field SuperPixel map (DRI-OCT),[12,13] or PanoMap (Cirrus OCT).[8] However, these two deviation maps used the normative database of narrow areas based on a uniform size and angle.

Our study has several limitations. First, all enrolled patients were Korean, and only a single ethnicity was used to build the normative database. Second, patients with high myopia were excluded. A wide-field normative database for patients with high myopia is also needed. Third, as mentioned earlier, not all anatomic variables, such as vessel configuration,[22,23] were controlled. Finally, it would be more logical to consider including analysis of the vascular arcade, as the RNFL passes along that region. This effect was not reflected in this study because only raw data for the thickness of each layer was used for analysis.

In conclusion, we constructed a wide-field normative database. Basic analyses were conducted to

translational vision science & technology

determine the parameter (RNFL, GCIPL, and GCC) and area that would have advantages in diagnosing glaucoma using this wide-field normative database. Based on this, a wide-field deviation map will be constructed in a future study, and it is expected to be more useful for the diagnosis of glaucoma.

Acknowledgments

Disclosure: **H. Kim,** (N); **J.S. Lee,** (N); **H.M. Park,** (N); **H. Cho,** (N); **H.W. Lim,** (N); **M. Seong,** (N); **J. Park,** (N); **W.J. Lee,** (N)

References

1. Lee EJ, Kim TW, Weinreb RN, et al. Trend-based analysis of retinal nerve fiber layer thickness measured by optical coherence tomography in eyes with localized nerve fiber layer defects. *Invest Ophthalmol Vis Sci*. 2011;52(2):1138–1144.

2. Leung CK. Diagnosing glaucoma progression with optical coherence tomography. *Curr Opin Ophthalmol*. 2014;25(2):104–111.

3. Leung CK, Cheung CY, Weinreb RN, et al. Evaluation of retinal nerve fiber layer progression in glaucoma: a study on optical coherence tomography guided progression analysis. *Invest Ophthalmol Vis Sci*. 2010;51(1):217–222.

4. Wollstein G, Schuman JS, Price LL, et al. Optical coherence tomography longitudinal evaluation of retinal nerve fiber layer thickness in glaucoma. *Arch Ophthalmol*. 2005;123(4):464–470.

5. Kim KE, Park KH. Macular imaging by optical coherence tomography in the diagnosis and management of glaucoma. *Br J Ophthalmol*. 2018;102(6):718–724.

6. Hood DC, Raza AS, de Moraes CG, et al. Glaucomatous damage of the macula. *Prog Retin Eye Res*. 2013;32:1–21.

7. Lee WJ, Kim YK, Park KH, Jeoung JW. Trend-based analysis of ganglion cell-inner plexiform layer thickness changes on optical coherence tomography in glaucoma progression. *Ophthalmology*. 2017;124(9):1383–1391.

8. Lee WJ, Kim TJ, Kim YK, et al. Serial combined wide-field optical coherence tomography maps for detection of early glaucomatous structural progression. *JAMA Ophthalmol*. 2018;136(10):1121–1127.

9. Lee WJ, Na KI, Ha A, et al. Combined use of retinal nerve fiber layer and ganglion cell-inner plexiform layer event-based progression analysis. *Am J Ophthalmol*. 2018;196:65–71.

10. Kim YK, Ha A, Na KI, et al. Temporal relation between macular ganglion cell-inner plexiform layer loss and peripapillary retinal nerve fiber layer loss in glaucoma. *Ophthalmology*. 2017;124(7):1056–1064.

11. Kim YK, Jeoung JW, Park KH. Inferior macular damage in glaucoma: its relationship to retinal nerve fiber layer defect in macular vulnerability zone. *J Glaucoma*. 2017;26(2):126–132.

12. Lee WJ, Oh S, Kim YK, et al. Comparison of glaucoma-diagnostic ability between wide-field swept-source OCT retinal nerve fiber layer maps and spectral-domain OCT. *Eye (Lond)*. 2018;32(9):1483–1492.

13. Lee WJ, Na KI, Kim YK, et al. Diagnostic ability of wide-field retinal nerve fiber layer maps using swept-source optical coherence tomography for detection of preperimetric and early perimetric glaucoma. *J Glaucoma*. 2017;26(6):577–585.

14. Chen TC, Hoguet A, Junk AK, et al. Spectral-domain OCT: helping the clinician diagnose glaucoma: a report by the American Academy of Ophthalmology. *Ophthalmology*. 2018;125(11):1817–1827.

15. Ha A, Park KH. Optical coherence tomography for the diagnosis and monitoring of glaucoma. *Asia Pac J Ophthalmol (Phila)*, https://doi.org/10.22608/APO.201902. Online ahead of print.

16. Chauhan BC, Burgoyne CF. From clinical examination of the optic disc to clinical assessment of the optic nerve head: a paradigm change. *Am J Ophthalmol*. 2013;156(2):218–227.e2.

17. Anderson D, Patella V. *Automated Static Perimetry*. 2nd ed. St. Louis, MO: Mosby; 1999.

18. DeLong ER, DeLong DM, Clarke-Pearson DL. Comparing the areas under two or more correlated receiver operating characteristic curves: a nonparametric approach. *Biometrics*. 1988;44(3):837–845.

19. Hood DC. Improving our understanding, and detection, of glaucomatous damage: an approach

based upon optical coherence tomography (OCT). *Prog Retin Eye Res*. 2017;57:46–75.

20. Gabriele ML, Ishikawa H, Wollstein G, et al. Peripapillary nerve fiber layer thickness profile determined with high speed, ultrahigh resolution optical coherence tomography high-density scanning. *Invest Ophthalmol Vis Sci*. 2007;48(7):3154–3160.

21. Kaushik S, Pandav SS, Ichhpujani P, Gupta A. Fixed-diameter scan protocol preferable for retinal nerve fibre layer measurement by optical coherence tomography in all sizes of optic discs. *Br J Ophthalmol*. 2009;93(7):895–900.

22. Resch H, Pereira I, Hienert J, et al. Influence of disc-fovea angle and retinal blood vessels on interindividual variability of circumpapillary retinal nerve fibre layer. *Br J Ophthalmol*. 2016;100(4):531–536.

23. Chua J, Schwarzhans F, Nguyen DQ, et al. Compensation of retinal nerve fibre layer thickness as assessed using optical coherence tomography based on anatomical confounders. *Br J Ophthalmol*. 2020;104(2):282–290.

24. Mwanza JC, Lee G, Budenz DL. Effect of adjusting retinal nerve fiber layer profile to fovea-disc angle axis on the thickness and glaucoma diagnostic performance. *Am J Ophthalmol*. 2016;161:12–21.e1–2.

25. Amini N, Nowroozizadeh S, Cirineo N, et al. Influence of the disc-fovea angle on limits of RNFL variability and glaucoma discrimination. *Invest Ophthalmol Vis Sci*. 2014;55(11):7332–7342.

26. Qiu K, Chen B, Yang J, et al. Effect of optic disc-fovea distance on the normative classifications of macular inner retinal layers as assessed with OCT in healthy subjects. *Br J Ophthalmol*. 2019;103(6):821–825.

27. Chauhan BC, Sharpe GP, Hutchison DM. Imaging of the temporal raphe with optical coherence tomography. *Ophthalmology*. 2014;121(11):2287–2288.

28. Mayama C, Saito H, Hirasawa H, et al. Diagnosis of early-stage glaucoma by grid-wise macular inner retinal layer thickness measurement and effect of compensation of disc-fovea inclination. *Invest Ophthalmol Vis Sci*. 2015;56(9):5681–5690.

translational vision science & technology